Physics Letters B 792 (2019) 470–475

Contents lists available at ScienceDirect

Physics Letters B

www.elsevier.com/locate/physletb

Orientation dependence of confinement-deconfinement phase transition in anisotropic media

Irina Aref'eva [a], Kristina Rannu [b,*], Pavel Slepov [c]

[a] Steklov Mathematical Institute, Russian Academy of Sciences, Gubkina str. 8, 119991, Moscow, Russia
[b] Peoples Friendship University of Russia, Miklukho-Maklaya str. 6, 117198, Moscow, Russia
[c] Moscow State University, Faculty of Physics, 1-2 Leninskie Gory, 119991, Moscow, Russia

ARTICLE INFO

Article history:
Received 31 December 2018
Received in revised form 2 April 2019
Accepted 5 April 2019
Available online 10 April 2019
Editor: M. Cvetič

Keywords:
AdS/QCD
Holography
Phase transition

ABSTRACT

We study the T-μ phase diagram of anisotropic media, created in heavy-ion collisions (HIC). Such a statement of the problem is due to several indications that this media is anisotropic just after HIC. To study T-μ phase diagram we use holographic methods. To take into account the anisotropy we use an anisotropic black brane solutions for a bottom-up QCD approach in 5-dim Einstein-dilaton-two-Maxwell model constructed in our previous work. We calculate the minimal surfaces of the corresponding probing open string world-sheet in anisotropic backgrounds with various temperatures and chemical potentials. The dynamical wall (DW) locations, providing the quark confinement, depend on the orientation of the quark pairs, that gives a crossover transition between confinement/deconfinement phases in the dual gauge theory.

1. Introduction

Study of the phase diagram in the temperature and chemical potential (μ, T)-plane is one of the most important questions for QCD [1]. It aims to describe the physics of strongly interacting matter at extreme energy densities, where we have evidence that a new phase of matter, the quark gluon-plasma (QGP) appears, as well to understand the matter, which prevailed in early Universe in first 30 micro seconds.

It is well known that perturbative methods are inapplicable to study this subject. The lattice QCD still has difficulties with the study of theories with non-zero chemical potential due to the sign problem [2]. The gravity/gauge duality provides an alternative tool to study T-μ phase diagram [3–5].

The phase diagram has been experimentally studied only for small μ and large T values (RHIC, LHC) on the one hand and for low energies (small T) and finite chemical potential values (SPS) on the other hand. The experimental study of the phase diagram in between these two particular cases is one of the main tasks of FAIR and NICA, now being under construction. For this purpose the results of the beam scanning in HIC are supposed to be analyzed. In this context note, that there is an obvious anisotropy (the nonequivalence of the longitudinal and transverse directions) in the substance produced in HIC. In fact it is believed, that QGP formed in HIC is initially in an anisotropic state and isotropization occurs approximately in $0.5 \div 2$ fm/c after a collision [6]. Therefore it seems natural to assume that the results of the beam scanning will study the phase transition in an anisotropic QCD (with parameter of anisotropy depending on time). One cannot use the anisotropic lattice QCD [9–12] to study T-μ phase diagram because of the well known sign problem mentioned above.

This anisotropy of QGP can be taken into account holographically. An additional argument to use anisotropic holographic model is that it supports the estimation of multiplicity [7]. We use the bottom-up holographic model to study T-μ phase diagram and investigate the anisotropy influence on it. On the gravity side anisotropy is supplied with the magnetic ansatz of Maxwell field to dilaton gravity action. Non-zero chemical potential is introduced via electric ansatz for the second Maxwell field [13]. Thereby the 5-dimensional dilaton gravity with two Maxwell fields turns out to be the most suitable model. Such model was considered in [13, 14]. The simplest anisotropic model, characterized by anisotropic parameter ν, has been investigated in [7]. The feature of this particular model is that it correctly reproduces the energy dependence of multiplicity of charged particles produced at LHC in heavy ion collisions (results by ATLAS and Alice [15,16]). Other holographic models cannot fit experimental data in spite of several attempts

* Corresponding author.
E-mail addresses: arefeva@mi.ras.ru (I. Aref'eva), rannu_ka@pfur.ru (K. Rannu), slepov@mi.ras.ru (P. Slepov).

https://doi.org/10.1016/j.physletb.2019.04.012

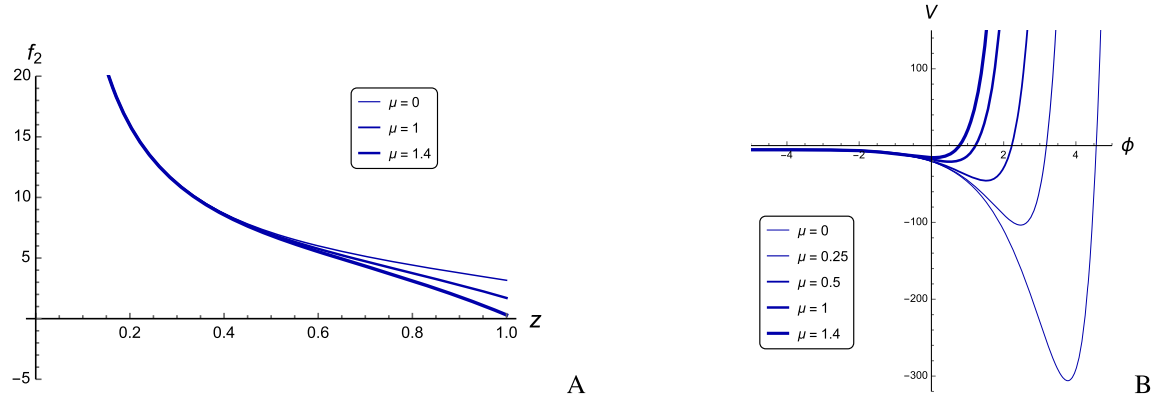

Fig. 1. A) Coupling function $f_2(z)$ for $z_h = 1$, $c = -1$, $q = 1$ and different μ in anisotropic case, $\nu = 4.5$. B) Scalar field potential $V(\phi)$ for $z_h = 1$, $c = -1$ and different μ in anisotropic case, $\nu = 4.5$.

(see our previous papers on the subject [7,8,13]). We take $\nu = 4.5$ to fit the experimental data.

The specific view of T-μ diagram describing the confinement/deconfinement phase transition in anisotropic media depends on orientation of the quark pair relative to the anisotropy axis. Anisotropy axis in QGP created in HIC is defined by the axes of ions collisions. In our previous work we studied longitudinal and transverse orientation cases and showed that they have two different T-μ curves on phase diagram [13]. But it is obvious that in real experiment, especially for large chemical potentials, the quark pair orientation should be random thus causing blurring of the phase transition line. In this paper we investigate the general confinement/deconfinement phase transition picture for arbitrary quark pair orientation and describe the emerging variety of scenarios.

We consider a 5-dim metric defined by anisotropic parameter ν, non-trivial warp-factor, non-zero time component of the first Maxwell field and non-zero longitudinal magnetic component of the second Maxwell field. We take the warp-factor in the simplest form $b(z) = e^{\frac{cz^2}{2}}$, as this particular case allows to construct explicit solution [13]. We study the confinement/deconfinement phase transition line for the pair of quarks in the anisotropic QGP. We show the dependence of the confinement/deconfinement phase transition on the angle θ between quarks line and heavy-ion collisions line. We calculate the expectation values of the rectangular temporal Wilson loop $W_{\theta T}$ for different orientation of the spacial part of the Wilson loop and find the conditions of the confinement/deconfinement phase transition for this line. For this purpose we introduce the effective potential $\mathcal{V}(z)$, that depends on the angle θ and describes the interquark interaction. The confinement takes place, when the effective potential $\mathcal{V}$ has a critical point. We find conditions, under which the critical point exists, and study the dependence of the confinement/deconfinement phase transition temperature on chemical potential μ and angle θ.

The specific feature of the holographic description of the confinement/deconfinement is the position of the phase diagram associated with the Wilson loop behavior relative to the line of the Hawking-Page phase transition, characterized by the 5-dim background metric. It is evident, that unlike the confinement/deconfinement transition line, the Hawking-Page transition line's position on the phase diagram doesn't depend on the angle θ. As a result the change of this angle leads to changing of the mutual arrangement of the confinement/deconfinement transition line and Hawking-Page transition line on the phase diagram. We find the critical value, for which the top of the Hawking-Page transition line, corresponding to $\mu = 0$, and the top of the confinement/deconfinement transition line coincide.

The paper is organized as follows. In Sect. 2 we briefly describe the 5-dim black brane solution in the anisotropic background (Sect. 2.1) and sketch calculates of the expectation value of the temporal Wilson loop (Sect. 2.2). In Sect. 3 we find the condition of the confinement-deconfinement phase transition for zero and non-zero temperature. In Sect. 4 we perform detailed phase diagrams depending on the angle θ and in Sect. 5 discuss further directions of investigation of holographic anisotropic QCD.

2. Setup

2.1. The model

We consider a 5-dimensional Einstein-dilaton-two-Maxwell system. In the Einstein frame the action of the system is specified as

$$S = \int \frac{d^5x}{16\pi G_5}\sqrt{-\det(g_{\mu\nu})} \times \left[R - \frac{f_1(\phi)}{4}F^2_{(1)} - \frac{f_2(\phi)}{4}F^2_{(2)} - \frac{1}{2}\partial_\mu\phi\partial^\mu\phi - V(\phi)\right], \quad (1)$$

where $F^2_{(1)}$ and $F^2_{(2)}$ are the squares of the Maxwell fields $F^{(1)}_{\mu\nu} = \partial_\mu A^{(1)}_\nu - \partial_\nu A^{(1)}_\mu$ and $F^{(2)}_{\mu\nu} = q\ dy^1 \wedge dy^2$, $f_1(\phi)$ and $f_2(\phi)$ are the gauge kinetic functions associated with the corresponding Maxwell fields, $V(\phi)$ is the potential of the scalar field ϕ.

To find the black brane solution in the anisotropic background we used the metric ansatz in the following form:

$$ds^2 = G_{\mu\nu}dx^\mu dx^\nu = \frac{L^2 b(z)}{z^2}\left[-g(z)dt^2 + dx^2 + z^{2-\frac{2}{\nu}}\left(dy_1^2 + dy_2^2\right) + \frac{dz^2}{g(z)}\right], \quad (2)$$

$$\phi = \phi(z), \qquad A^{(1)}_\mu = A_t(z)\delta^0_\mu, \quad (3)$$

$$F^{(2)}_{\mu\nu} = q\ dy^1 \wedge dy^2, \quad (4)$$

where $b(z)$ is the warp factor and $g(z)$ is the blackening function (see (2.31) and (2.38) in [13]); we set the AdS radius $L = 1$. The coupling function f_2, directly connected with the model anisotropy, depends on chemical potential as well (Fig. 1.A). The potential V (Fig. 1.B) can be approximated by a sum of two exponents and a negative constant (see (2.70)–(2.74) in [13]). Functions f_1 and f_2 are given by eqs. (2.17) and (2.51) in [13]. All the quantities in formulas and figures are presented in dimensionless units.

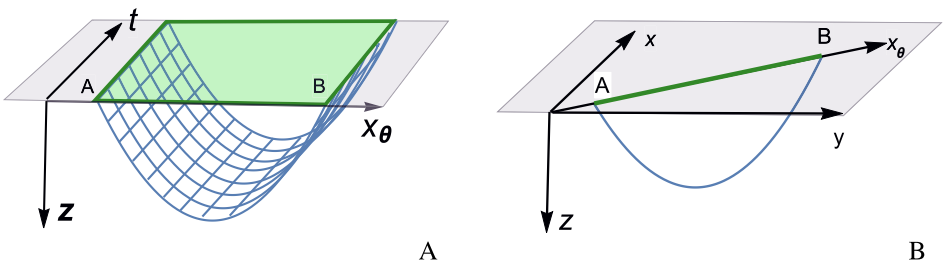

Fig. 2. A) Wilson loop and the world sheet. B) Projection of the world sheet to fixed t.

2.2. The Wilson loop

The purpose of our consideration is to calculate the expectation value of the temporal Wilson loop

$$W[C_\theta] = e^{-S_{\theta,T}}, \tag{5}$$

oriented along vector $\vec{n}$, such that $n_x = \cos\theta$, $n_y = \sin\theta$.

Following the holographic approach [18–20] we have to calculate the value of the Nambu-Goto action for the test string in our background:

$$S = -\frac{1}{2\pi\alpha'}\int dt\, d\xi\, e^{\sqrt{\frac{2}{3}}\phi(z)}\sqrt{-\det G_{\mu\nu}\partial_\alpha X^\mu \partial_\beta X^\nu}, \tag{6}$$

where $G_{\mu\nu}$ is given by (2). The world sheet presented in Fig. 2 is parameterized as

$$X^0 \equiv t, \quad X^1 \equiv x = \xi\cos\theta, \quad X^2 \equiv y_1 = \xi\sin\theta,$$
$$X^3 \equiv y_2 = \text{const}, \quad X^4 \equiv z = z(\xi).$$

The action (6) can be rewritten:

$$S = -\frac{\tau}{2\pi\alpha'}\int d\xi\; M(z(\xi))\sqrt{\mathcal{F}(z(\xi)) + (z'(\xi))^2}, \quad \tau = \int dt, \tag{7}$$

$$M(z(\xi)) = \frac{b(z(\xi))}{z(\xi)^2}\, e^{\sqrt{\frac{2}{3}}\phi(z)},$$

$$\mathcal{F}(z(\xi)) = g(z(\xi))\left(z(\xi)^{2-\frac{2}{\nu}}\sin^2(\theta) + \cos^2(\theta)\right). \tag{8}$$

Let us introduce the effective potential:

$$\mathcal{V}(z) \equiv M(z)\sqrt{\mathcal{F}(z)}. \tag{9}$$

From (7) we have representations for the character length of the string and the action:

$$\frac{\ell}{2} = \int_0^{z_*} \frac{1}{\sqrt{\mathcal{F}(z)}}\,\frac{dz}{\sqrt{\frac{\mathcal{V}^2(z)}{\mathcal{V}^2(z_*)} - 1}}, \tag{10}$$

$$\frac{S}{2} = \int_\epsilon^{z_*} \frac{\mathcal{V}(z)}{\mathcal{V}(z_*)}\,\frac{M(z)dz}{\sqrt{\frac{\mathcal{V}^2(z)}{\mathcal{V}^2(z_*)} - 1}}, \tag{11}$$

where z_* is a top point. Here we introduce the UV cut-off ϵ since M has singular behavior near $z \sim 0$:

$$M(z) \underset{z\sim 0}{\sim} \frac{M_0}{z^k}, \quad k \geq 1. \tag{12}$$

From (10) and (11) we see that S and ℓ make sense if the potential is a decreasing function in the interval $0 < z < z_*$,

$$\mathcal{V}(z) > \mathcal{V}(z_*), \quad 0 < z_* < z_{min}, \tag{13}$$

where z_{min} is the local minimum of $\mathcal{V}(z)$, $z_{min} < z_h$. We are interested in studying the asymptotics of S at large ℓ. To get $\ell \to \infty$ and $S \to \infty$ we have to take $z_* = z_{min}$. Indeed, substituting

$$\frac{\mathcal{V}^2(z)}{\mathcal{V}^2(z_{min})} = 1 + \mathcal{V}_2(z - z_{min})^2 + o((z - z_{min})^2),$$
$$\mathcal{V}_2 \equiv \frac{\mathcal{V}''(z_{min})}{\mathcal{V}(z_{min})}, \tag{14}$$

into (10) and (11), we get

$$\ell = 2\int_0^{z_{min}} \frac{dz}{\sqrt{\mathcal{F}(z)\,\mathcal{V}_2}\,(z_{min} - z)}$$
$$\sim \sqrt{\frac{\mathcal{V}(z_{min})}{\mathcal{F}(z_{min})\,\mathcal{V}''(z_{min})}}\,\log(z_{min} - z), \tag{15}$$

$$S = 2\int_\epsilon^{z_{min}} \frac{\mathcal{V}(z)M(z)dz}{\mathcal{V}(z_{min})\sqrt{\mathcal{V}_2}\,(z_{min} - z)}$$
$$\sim M(z_{min})\sqrt{\frac{\mathcal{V}(z_{min})}{\mathcal{V}''(z_{min})}}\,\log(z_{min} - z), \tag{16}$$

so that $\ell \to \infty$ as $z \to z_{min} - 0$ and $S \to \infty$ as $z \to z_{min} - 0$.

The stationary point, $\mathcal{V}'|_{z=z_{min}} = 0$, is usually called a dynamical wall (DW) point and satisfies the equation:

$$z = z_{DW}: \quad \frac{M'(z)}{M(z)} + \frac{1}{2}\frac{\mathcal{F}'(z)}{\mathcal{F}(z)} = 0. \tag{17}$$

Taking the top point $z_* = z_{DW}$, we get

$$S \sim \sigma_{DW}\,\ell, \qquad \sigma_{DW} = M(z_{DW})\sqrt{\mathcal{F}(z_{DW})}. \tag{18}$$

3. Confinement/deconfinement phase transition

In our case the effective potential depends on the warp factor, the scalar field and the angle. To find stationary points of $\mathcal{V}(z)$ we solve the equation (17) for the potential (9) with arbitrary angle. This equation has the form

$$\Sigma(z, z_h, \mu, c, \nu) - \Theta(z, \nu, \theta) = 0, \tag{19}$$

where $\Sigma(z, z_h, \mu, c, \nu)$ does not depend on θ:

$$\Sigma(z, z_h, \mu, c, \nu) \equiv \sigma(z, c, \nu) + \frac{g'(z)}{2g(z)},$$
$$\sigma(z, c, \nu) \equiv cz + \frac{1}{\nu z}\sqrt{\frac{2}{3}}\sqrt{3c\,\nu^2 z^2\left(\frac{cz^2}{2} - 3\right) + 4\nu - 4}, \tag{20}$$

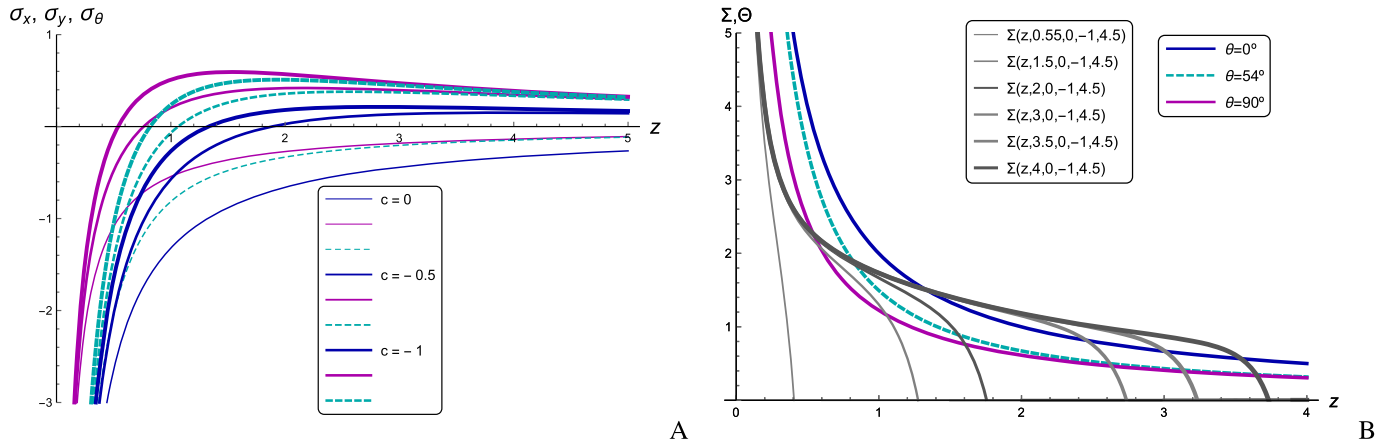

Fig. 3. A) Functions $\sigma_x(z,c,\nu)$ (blue lines), $\sigma_y(z,c,\nu)$ (magenta lines), $\sigma_\theta(z,c,\nu,\theta)$ (cyan dashed lines) for the angle $\theta = 54°$, $\nu = 4.5$ and for different c. B) DWs' positions, corresponding to the Wilson lines W_{xT}, W_{yT}, $W_{\theta T}$ in the anisotropic case $\nu = 4.5$, are given by intersections of gray lines representing $\Sigma(z)$ and the blue, cyan, magenta lines representing another part of the equation (19) for angles $\theta = 0°, 54°, 90°$. Here we vary z_h and c. In all cases to get the DW position we take the minimal intersection point.

and $\Theta(z,\nu,\theta)$ does:

$$\Theta(z,\nu,\theta) \equiv \frac{2}{z} - \frac{\left(1-\frac{1}{\nu}\right) z^{1-\frac{2}{\nu}} \sin^2(\theta)}{\cos^2(\theta) + z^{2-\frac{2}{\nu}} \sin^2(\theta)}. \tag{21}$$

Equations for DWs in particular cases for $\theta = 0, \pi/2$, considered previously in [13], follow immediately from equation (19). For zero temperature, i.e. $g = 1$, we get equation

$$\sigma_\theta(z,c,\nu) \equiv \sigma(z,c,\nu) - \Theta(z,\nu,\theta) = 0. \tag{22}$$

The existence/non-existence of solutions of equations (22) and (19) can be seen graphically at Fig. 3. At Fig. 3.A plots of $\sigma_x = \sigma_{\theta=0}$, $\sigma_y = \sigma_{\theta=\pi/2}$ and $\sigma_\theta(z,c,\nu,\theta)$ for a particular $\theta = 54°$ are presented. We see that for $c = 0$ there are no roots of equation (22), meanwhile there are roots for any orientations of the Wilson line and negative c presented here.

For non-zero temperature it is more convenient to find the roots of equation (19) by drawing $\Sigma(z,z_h,\mu,c,\nu)$ and $\Theta(z,\nu,\theta)$ separately and find their intersections. In this case the location of $\Theta(z,\nu,\theta)$ depends on the geometry of quark-antiquark pair, meanwhile the location of $\Sigma(z,z_h,\mu,c,\nu)$ depends on z_h, μ, c, ν. We see that for these parameters fixed the intersection of $\Sigma(z,z_h,\mu,c,\nu)$ and $\Theta(z,\nu,\theta)$ depends on the orientation. In particular, the line $\Sigma(z,1.5,0,-1,4.5)$ at Fig. 3.B intersects the magenta line and does not intersect the dashed darker cyan and blue lines. This shows that for $\theta = 90°$ confinement occurs, but for $\theta = 54°$ and, moreover, for $\theta = 0°$, does not. The disappearance of the root we interpret as disappearance of confinement. The parameters, at which this occurs, define the location of the Wilson confinement/deconfinement transition line. Since we are interested in location of the confinement/deconfinement line in the (μ,T)-plane, we use the expression for the temperature $T(z_h,\mu,c,\nu)$ given by formula (3.1) in [13]. The locations of the Wilson confinement/deconfinement transition lines on the (μ,T)-plane are presented at Fig. 4 by solid lines. We see that varying θ for chemical potential μ large enough we get essential spread of position of the confinement/deconfinement transition lines.

For small chemical potentials the situation is more complicated due to the Hawking-Page instability of the background (2) [13]. If the system cools down with the non-zero chemical potential less than some critical value μ_{cr}, the background at the temperature $T_{BB}(\mu)$ undergoes the phase transition from a large to a small black hole. This is a generalization of the corresponding effect in the isotropic case [21–25]. For zero μ the Hawking-Page phase transition takes place at T_{HP}, where the free energy equals zero and the black hole dissolves to thermodynamically stable thermal gas. The particular value of T_{HP} depends on parameters c and ν. For the isotropic background the Hawking-Page transition temperature T_{HP} is higher than for the anisotropic one with the same $c < 0$, also the temperature of the large/small black hole phase transition in the isotropic case is higher than in the anisotropic one, i.e. $T_{BB}^{(anis)}(\mu) < T_{BB}^{(iso)}(\mu)$. The value of the critical chemical potential, up to which this phase transition exists, in the anisotropic case is larger compared to the isotropic one, $\mu_{cr}^{(anis)} > \mu_{cr}^{(iso)}$. Also in [13] we have found that the point $(\mu_{cr}^{(anis)}, T_{cr}^{(anis)})$ for $\nu \to 1$ goes smoothly to $(\mu_{cr}^{(iso)}, T_{cr}^{(iso)})$. The location of the Hawking-Page transition line for anisotropic case $\nu = 4.5$ is presented at Fig. 4 by the dashed red line. This line starts at $(0, T_{HP})$ and end up at $(\mu_{cr}^{(anis)}, T_{cr}^{(anis)})$.

4. Results

The phase diagram in (μ,T)-plane is in fact defined by the relative disposition of the Hawking-Page transition line and the Wilson transition line. In the model we have determined the critical angles $\theta_{cr1} = 45°$, $\theta_{cr2} = 54°$ and $\theta_{cr3} = 65°$. For the critical angle $\theta_{cr1} = 45°$ the Hawking-Page phase transition line (red dashed line in Fig. 4) and the phase transition line, determined by the Wilson loop (orange line in Fig. 4), have only one common point $(\mu_{cr}^{(anis)}, T_{cr}^{(anis)})$ at the end of the Hawking-Page transition line. In this case for $\mu \le \mu_{cr}^{(anis)}$ the whole Hawking-Page line determines the confinement/deconfinement phase transition. For the angle $\theta_{cr2} = 54°$ the top point (corresponding to $\mu = 0$) of the Hawking-Page phase transition coincides with the top point of the Wilson phase transition (gray line in Fig. 4), $T_{HP} = T_{\text{top},\theta_{cr2}}$. For $\theta_{cr3} = 65°$ the Hawking-Page phase transition line and phase transition line, determined by the Wilson loop (red solid line), have only one common point $(\mu_{cr}^{(anis)}, T_{cr}^{(anis)})$ at the end of the Hawking-Page phase transition line again. In this case the whole confinement/deconfinement phase transition line is determined by the Wilson loop only since this line is located below the Hawking-Page phase transition line.

Between these critical values of θ we have the following pictures.

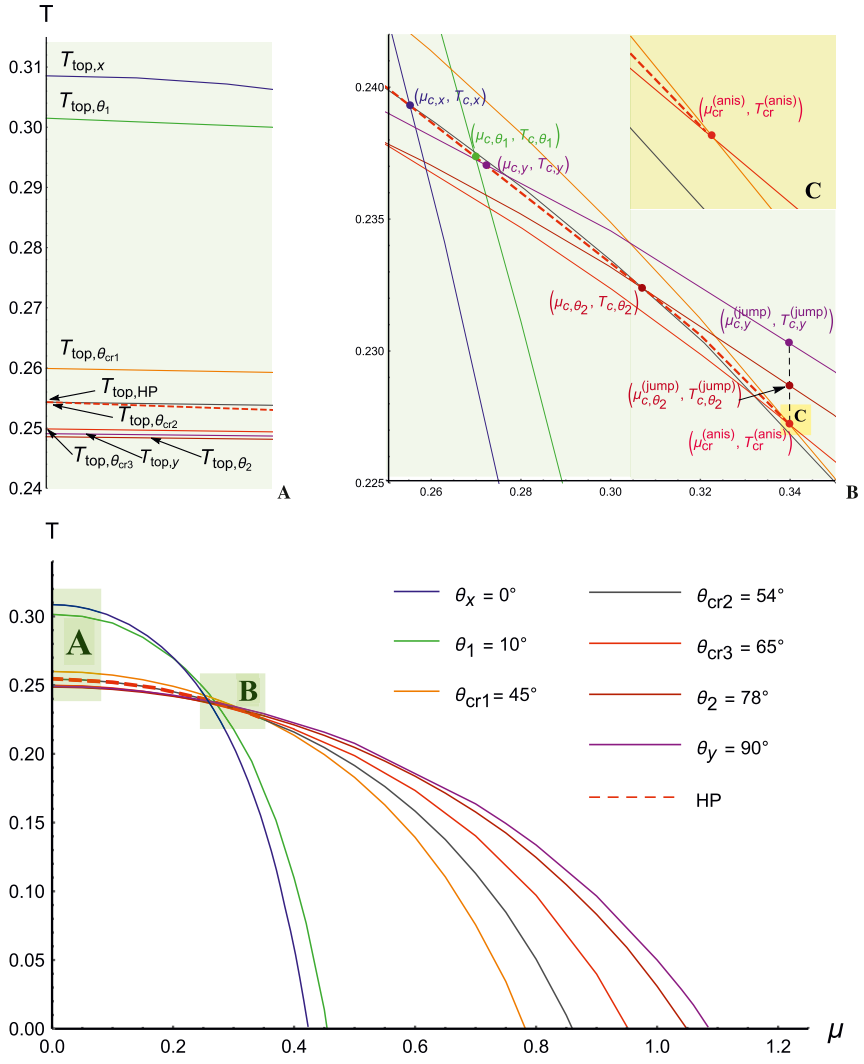

Fig. 4. Phase transition diagrams. The plots A) and B) are the zooms of the green areas and C) is a zoom of the yellow area in B).

- For $0° \leq \theta < 45°$ parts of the Wilson transition lines near zero values of the chemical potential enter the instability regions of our background, where the small black holes collapse to large ones. Here the phase transition is determined by the Hawking-Page phase transition. After the chemical potential exceeds some critical value, the confinement/deconfinement phase transition is no longer determined by the background and the influence on the Wilson loop starts to dominate, analogous to the longitudinal orientation case, presented as W_{xT} in [13] and associated with $\theta_x = 0°$. The green line on Fig. 4 corresponds to $\theta_1 = 10°$ and shows a typical disposition of the Wilson transition line in respect to the Hawking-Page transition line. It intersects the Hawking-Page line at the green point $(\mu_{c,\theta_1}, T_{c,\theta_1})$ shown at Fig. 4.B. The intersection of the Hawking-Page line with the Wilson transition line corresponding to $\theta_x = 0°$ is shown by the blue point at Fig. 4.B. While increasing the angle up to $\theta_{cr1} = 45°$, the intersection reaches the end point of the Hawking-Page transition line, $(\mu_{cr}^{(anis)}, T_{cr}^{(anis)})$.
- For $\theta_{cr1} = 45°$ the line corresponding to the Wilson loop contribution meets the Hawking-Page phase transition line at its very end (red point $(\mu_{cr}^{(anis)}, T_{cr}^{(anis)})$ on Fig. 4.B).
- For $45° < \theta < 54°$ we have no intersections of the Hawking-Page phase transition line and the Wilson transition line lies above, so there is a jump from the Hawking-Page to the Wilson transition line.
- For $\theta_{cr2} = 54°$ the Wilson line on the phase diagram (gray line) starts at $\mu = 0$ at the same point as the Hawking-Page transition line, then goes above it and intersects it again. Note that the gray line almost coincides with the Hawking-Page phase transition line (the dashed red line) at Fig. 4.
- For $54° < \theta < 65°$ we have no intersections of the Hawking-Page phase transition line and the Wilson transition line. In this case the whole confinement/deconfinement phase transition is determined by the Wilson transition line.
- For $\theta_{cr3} = 65°$ the line corresponding to the Wilson transition line meets the Hawking-Page phase transition line at its very end again (red point $(\mu_{cr}^{(anis)}, T_{cr}^{(anis)})$ on Fig. 4.B).
- For $65° < \theta \leq 90°$ the picture is analogous to the case of the transversal orientation case, presented as W_{yT} in [13] and corresponding to $\theta_y = 90°$. The confinement/deconfinement phase transition is determined by the Wilson transition line starting from the zero values of chemical potential up to $\mu_{c,y}$ (magenta point $(\mu_{c,y}, T_{c,y})$ on Fig. 4.B), where it meets the instability of the background. Starting from this point the Hawking-Page phase transition takes place up to $(\mu_{cr}^{(anis)}, T_{cr}^{(anis)})$, where we have a jump to a point $(\mu_{c,y}^{(jump)}, T_{c,y}^{(jump)})$ on the Wilson transition

line. A typical Wilson transition line for $\theta_2 = 78^\circ$ is presented in darker red. It intersects the Hawking-Page line in point $(\mu_{c,\theta_2}, T_{c,\theta_2})$, and the jump from the end of the Hawking-Page line $(\mu_{cr}^{(anis)}, T_{cr}^{(anis)})$ into the darker red point $(\mu_{c,\theta_2}^{(jump)}, T_{c,\theta_2}^{(jump)})$ is also shown on Fig. 4.B.

5. Conclusion and discussion

We have found the dependence of the confinement/deconfinement phase transition line on the orientation of the quark pair. For this purpose we have studied the behavior of the temporal Wilson loops in the particular 5-dimensional anisotropic background supported by dilaton and two-Maxwell field constructed in [13]. We specified the quark pair orientation by angle θ. For each angle there is its own confinement/deconfinement transition line (see a variety of these lines in Fig. 4). There is a Hawking-Page instability in our background. Combining the phase transition for the Wilson line with this Hawking-Page instability we have arrived to the picture presented in Fig. 4.

At the end we would like to point out, that the possibility of an experimental check of our estimation of the confinement/deconfinement line blurring essentially depends on the ability of the experimental measurement particle yield immediately after HIC. The reason for this is that the anisotropy effects are expected in the contents of the fireball, created in HIC, just after collision at times of about $0.5 \div 2$ fm/c. Anisotropy makes spectrum of the hadrons created by this fireball depend on the orientation, but this anisotropy disappears very soon and as a consequence the blurring disappears as well.

As to the future investigations, the following natural questions to static and non-static properties of our model are worth noting. As has been mentioned, the anisotropic background constructed in [13] can be generalized to provide a more realistic model. In this case the solution can be given in terms of quadratures only and we suppose to generalize the Wilson loop calculations to this more realistic case. As to static properties, it is natural to

- investigate θ-oriented Wilson loops based on more complicated factor $b(z)$, in particular such that in the isotropic limit it fits the Cornell potential known by lattice QCD;
- study the Regge spectrum for mesons, adding the probe gauge fields to the backgrounds and find its dependence on θ;
- consider estimations for direct photons and find dependence on orientation [14];
- evaluate transport coefficients and their dependence on the anisotropy;
- estimate the holographic entanglement entropy and find its dependence on θ; note that this has been done in [7] for zero chemical potential and $\theta = 0, \pi/2$; the isotropic case for non-zero chemical potential has been considered recently in [26];
- find a generalization results of [17] where an explicit isotropic solution for the dilaton potential as a sum of two exponents and zero chemical potential has been found.

As to the thermalization processes, which are the main motivations of our consideration of the anisotropic background (see details in [14,27]), it would be interesting to investigate the behavior of the temporal Wilson loop during thermalization. This problem for zero chemical potential has been studied in [28]. It is also interesting to generalize the result of paper [29] and consider thermalization of the spacial Wilson loops for non-zero chemical potential. This will give the dependence of the drag-forces on the chemical potential.

Acknowledgements

This work was partially (I.A. and P.S.) supported by the "BASIS" Science Foundation (grant No. 18-1-1-80-4).

References

[1] A. Andronic, P. Braun-Munzinger, K. Redlich, J. Stachel, Decoding the phase structure of QCD via particle production at high energy, Nature 561 (7723) (2018) 321, arXiv:1710.09425 [nucl-th].
[2] G. Aarts, in: Proceedings, 13th International Workshop on Hadron Physics, Angra dos Reis, Rio de Janeiro, Brazil, March 22–27, 2015, J. Phys. Conf. Ser. 706 (2016) 022004, arXiv:1512.05145 [hep-lat].
[3] J. Casalderrey-Solana, H. Liu, D. Mateos, K. Rajagopal, U.A. Wiedemann, Gauge/String Duality, Hot QCD and Heavy Ion Collisions, Cambridge University Press, 2014, arXiv:1101.0618 [hep-th].
[4] I.Ya. Aref'eva, Holographic approach to quark-gluon plasma in heavy ion collisions, Phys. Usp. 57 (2014) 527.
[5] O. DeWolfe, S.S. Gubser, C. Rosen, D. Teaney, Heavy ions and string theory, Prog. Part. Nucl. Phys. 75 (2014) 86, arXiv:1304.7794 [hep-th].
[6] M. Strickland, Thermalization and isotropization in heavy-ion collisions, Pramana 84 (2015) 671.
[7] I.Ya. Aref'eva, A.A. Golubtsova, E. Gourgoulhon, Analytic black branes in Lifshitz-like backgrounds and thermalization, J. High Energy Phys. 1609 (2016) 142, arXiv:1601.06046 [hep-th].
[8] I.Ya. Aref'eva, Holography for heavy-ion collisions at LHC and NICA. Results of the last two years, EPJ Web Conf. 191 (2018) 05010.
[9] F. Karsch, SU(N) gauge theory couplings on asymmetric lattices, Nucl. Phys. B 205 (1982) 285.
[10] F. Karsch, I. Stamatescu, QCD thermodynamics with light quarks. Quantum corrections to the fermionic anisotropy parameter, Nucl. Phys. B 227 (1989) 153.
[11] I.Y. Arefeva, Regge regime in QCD and asymmetric lattice gauge theory, Phys. Lett. B 325 (1994) 171, arXiv:hep-th/9311115.
[12] P. de Forcrand, W. Unger, H. Vairinhos, Strong-coupling lattice QCD on anisotropic lattices, Phys. Rev. D 97 (2018) 034512, arXiv:1710.00611 [hep-lat].
[13] I. Aref'eva, K. Rannu, Holographic anisotropic background with confinement-deconfinement phase transition, J. High Energy Phys. 5 (2018) 206, arXiv:1802.05652 [hep-th].
[14] I.Ya. Aref'eva, Holography for heavy ions collisions at LHC and NICA, EPJ Web Conf. 164 (2017) 01014, arXiv:1612.08928 [hep-th].
[15] G. Aad, et al., ATLAS Collab., Measurement of the centrality dependence of the charged particle pseudorapidity distribution in lead-lead collisions at $\sqrt{s_{NN}} = 2.76$ TeV with the ATLAS detector, Phys. Lett. B 170 (2012) 363, arXiv:1108.6027 [hep-ex].
[16] J. Adam, et al., ALICE Collab., Centrality dependence of the charged-particle multiplicity density at mid-rapidity in Pb-Pb collisions at $\sqrt{s_{NN}} = 5.02$ TeV, Phys. Rev. Lett. 116 (2016) 222302, arXiv:1512.06104 [nucl-ex].
[17] I.Ya. Aref'eva, A.A. Golubtsova, G. Policastro, Exact holographic RG flows and the $A_1 \times A_1$ Toda chain, arXiv:1803.06764 [hep-th].
[18] J.M. Maldacena, Wilson loops in large N field theories, Phys. Rev. Lett. 80 (1998) 4859, arXiv:hep-th/9803002.
[19] S.J. Rey, S. Theisen, J.T. Yee, Wilson-Polyakov loop at finite temperature in large-N gauge theory and anti-de Sitter supergravity, Nucl. Phys. B 527 (1998) 171, arXiv:hep-th/9803135.
[20] A. Brandhuber, N. Itzhaki, J. Sonnenschein, S. Yankielowicz, High energy physics – theory Wilson loops in the large N limit at finite temperature, Phys. Lett. B 434 (1998) 36, arXiv:hep-th/9803137.
[21] A. Chamblin, R. Emparan, C.V. Johnson, R.C. Myers, Charged AdS black holes and catastrophic holography, Phys. Rev. D 60 (1999) 064018, arXiv:hep-th/9902170.
[22] O. DeWolfe, S.S. Gubser, C. Rosen, A holographic critical point, Phys. Rev. D 83 (2011) 086005, arXiv:1012.1864 [hep-th].
[23] O. DeWolfe, S.S. Gubser, C. Rosen, Dynamic critical phenomena at a holographic critical point, Phys. Rev. D 84 (2011) 126014, arXiv:1108.2029 [hep-th].
[24] S. He, S.-Y. Wu, Y. Yang, P.-H. Yuan, Phase structure in a dynamical soft-wall holographic QCD model, J. High Energy Phys. 04 (2013) 093, arXiv:1301.0385 [hep-th].
[25] Y. Yang, P.-H. Yuan, Confinement-deconfinement phase transition for heavy quarks in a soft wall holographic QCD model, J. High Energy Phys. 1512 (2015) 161, arXiv:1506.05930 [hep-th].
[26] D. Dudal, S. Mahapatra, Interplay between the holographic QCD phase diagram and entanglement entropy, J. High Energy Phys. 07 (2018) 120, arXiv:1805.02938 [hep-th].
[27] I. Aref'eva, Multiplicity and theremalization time in heavy-ions collisions, EPJ Web Conf. 125 (2016) 01007.
[28] A. Hajilou, M. Ali-Akbari, F. Charmchi, A classical string in Lifshitz-Vaidya geometry, EPJ C 78 (2018) 424, arXiv:1707.00967 [hep-th].
[29] D.S. Ageev, I.Ya. Aref'eva, A.A. Golubtsova, E. Gourgoulhon, Thermalization of holographic Wilson loops in spacetimes with spatial anisotropy, NUPHB14333, arXiv:1606.03995 [hep-th], 2018.